Infrared absorption of gaseous CH2BrOO detected with a step-scan Fourier-transform absorption spectrometer

Yu-Hsuan Huang and Yuan-Pern Lee

Citation: The Journal of Chemical Physics **141**, 164302 (2014); doi: 10.1063/1.4897982
View online: http://dx.doi.org/10.1063/1.4897982
View Table of Contents: http://scitation.aip.org/content/aip/journal/jcp/141/16?ver=pdfcov
Published by the AIP Publishing

Infrared absorption of gaseous CH_2BrOO detected with a step-scan Fourier-transform absorption spectrometer

Yu-Hsuan Huang[1] and Yuan-Pern Lee[1,2,a)]
[1]*Department of Applied Chemistry and Institute of Molecular Science, National Chiao Tung University, Hsinchu 30010, Taiwan*
[2]*Institute of Atomic and Molecular Sciences, Academia Sinica, Taipei 10617, Taiwan*

(Received 21 August 2014; accepted 1 October 2014; published online 22 October 2014)

CH_2BrOO radicals were produced upon irradiation, with an excimer laser at 248 nm, of a flowing mixture of CH_2Br_2 and O_2. A step-scan Fourier-transform spectrometer coupled with a multipass absorption cell was employed to record temporally resolved infrared (IR) absorption spectra of reaction intermediates. Transient absorption with origins at 1276.1, 1088.3, 961.0, and 884.9 cm^{-1} are assigned to ν_4 (CH_2-wagging), ν_6 (O–O stretching), ν_7 (CH_2-rocking mixed with C–O stretching), and ν_8 (C–O stretching mixed with CH_2-rocking) modes of *syn*-CH_2BrOO, respectively. The assignments were made according to the expected photochemistry and a comparison of observed vibrational wavenumbers, relative IR intensities, and rotational contours with those predicted with the B3LYP/aug-cc-pVTZ method. The rotational contours of ν_7 and ν_8 indicate that hot bands involving the torsional (ν_{12}) mode are also present, with transitions $7_0^1 12_v^v$ and $8_0^1 12_v^v$, v = 1–10. The most intense band (ν_4) of *anti*-CH_2BrOO near 1277 cm^{-1} might have a small contribution to the observed spectra. Our work provides information for directly probing gaseous CH_2BrOO with IR spectroscopy, in either the atmosphere or laboratory experiments. © *2014 AIP Publishing LLC*. [http://dx.doi.org/10.1063/1.4897982]

I. INTRODUCTION

Bromomethylperoxy radical (CH_2BrOO) is an important intermediate in the oxidation of brominated methanes in the atmosphere, especially in marine regions.[1–5] Initiation of the oxidation proceeds via abstraction of a hydrogen atom of CH_3Br, which is the main source of stratospheric bromine,[6] by OH or Cl to form the CH_2Br radical.[7,8] The CH_2Br radical reacts readily with ambient O_2 to form the CH_2BrOO radical.[9,10] The main decay processes of CH_2BrOO radical would be either its self-reaction[11,12] or reaction with other atmospheric constituents such as NO[13] and HO_2.[11] These reactions might lead to the production of free bromine atoms that are engaged in the depletion of stratospheric ozone with high efficiency. [14–16]

Nielsen *et al.* reported UV absorption spectrum of the $\tilde{B}^2A'' \leftarrow \tilde{X}^2A''$ transition of the gaseous CH_2BrOO radical, produced from the reaction of F + CH_3Br in O_2 using pulse radiolysis.[12] The spectrum was later revised because of partial interference by the absorption of the CH_3Br-F adduct.[17] The revised spectrum agrees satisfactorily with that reported by Villenave and Lesclaux,[11] who employed the reaction Cl + CH_3Br in O_2 to produce gaseous CH_2BrOO radicals. The spectrum resembles those of most alkyl and halogen-substituted alkylperoxy radicals, showing a broad feature without structure with a maximal cross section of $\sigma = (3.59 \pm 0.11) \times 10^{-18}$ cm^2 $molecule^{-1}$ at 240 nm. This reported cross section was used to monitor the concentration of CH_2BrOO in the study of its self-reaction,

$$CH_2BrOO + CH_2BrOO \rightarrow 2CH_2BrO + O_2 \text{ and other products,} \quad (1)$$

to determine a rate coefficient of $k_1 = (1.1 \pm 0.4) \times 10^{-12}$ cm^3 $molecule^{-1}s^{-1}$ at 298 K.[11] The CH_2BrO thus formed is reported to undergo subsequent unimolecular decomposition,[18,19]

$$CH_2BrO \rightarrow H_2CO + Br. \quad (2)$$

The end products observed for the self-reaction of CH_2BrOO are H_2CO, CO, and H(Br)CO.[12,18]

As the intense UV absorption of the $\tilde{B} \leftarrow \tilde{X}$ transition employed in kinetic investigations has no distinct structure, selective detection among various alkylperoxy radicals is precluded. Even though the $\tilde{A} \leftarrow \tilde{X}$ transition of CH_2BrOO is expected to have some vibronic progressions, similar to those reported for CH_3OO and CD_3OO,[20] this transition is expected to be weak; no observation of the $\tilde{A} \leftarrow \tilde{X}$ transition of CH_2BrOO has been reported. There is no report of the infrared (IR) or microwave spectrum of CH_2BrOO.

We have demonstrated that time-resolved Fourier-transform infrared (FTIR) absorption spectra of transient intermediates in gaseous reactions can be detected with a step-scan Fourier-transform infrared spectrometer coupled with a multipass absorption cell.[21,22] The IR absorption spectra of several alkylperoxy radicals, such as CH_3OO,[23] *cis*-$CH_3C(O)OO$ and *trans*-$CH_3C(O)OO$,[24] and *cis*-$C_6H_5C(O)OO$,[25] have been identified with this method. Here, we report an application of this technique to record the IR absorption spectra of gaseous CH_2BrOO radical.

a)Author to whom correspondence should be addressed. Electronic mail: yplee@mail.nctu.edu.tw. Fax: 886-3-5713491.

II. EXPERIMENTS

Detailed description of our experimental setup has been published previously.[21] Briefly, a White cell with a base path of length 15 cm and an effective path of length 3.6 m was placed in the external port of a step-scan Fourier-transform spectrometer (Bruker, Vertex 80v). The White cell, of volume ~1.4 L, accommodates two rectangular quartz windows (3×12 cm^2) to pass photolysis beams that propagate perpendicularly to multi-passing IR beams. A KrF excimer laser (Lambda Physik, CompexPro 102F, 11 Hz, ~176 mJ pulse^{-1}, beam size 1.3×0.9 cm^2) emitting at 248 nm passed through these quartz windows and was reflected six times with two external laser mirrors to photodissociate a flowing mixture of CH_2Br_2 and O_2.

We obtained temporally resolved difference absorption spectra from interferograms recorded consecutively with ac- and dc-coupled signals. The preamplified ac- and dc-coupled signals from the MCT detector were sent directly to the internal 24-bit analogue-to-digital converter (ADC) of the spectrometer. Typically, 100 data points were acquired at 12.5-μs integrated intervals for a period 1250 μs after photolysis; the signal was typically averaged over 15 laser shots at each scan step. With appropriate optical filters to define a narrow spectral region, we performed undersampling to decrease the number of points in the interferogram, hence the duration of data acquisition. For spectra in the range 800–3949 cm^{-1} at resolution 4.0 cm^{-1}, 1999 scan steps were completed within ~1 h. For spectra in the range 800–1500 cm^{-1} at resolution 0.5 cm^{-1}, 3046 scan steps were completed within ~1.5 h. To improve further the ratio of signal to noise, we recorded and averaged nine sets of data under similar experimental conditions. The instrumental resolution is listed in the text unless otherwise noted; the effective full-width at half-maximum (FWHM) after apodization with the Blackman-Harris 3-Term function is ~128% of the listed instrumental resolution.

O_2 was employed as both a reactant and an efficient quencher. A stream of N_2 was bubbled through liquid CH_2Br_2 before entering the reactor. Experimental conditions were as follows: flow rates $F_{CH_2Br_2} \cong 0.07$, $F_{N_2} \cong 0.2$ and $F_{O_2} \cong 23.7$ STP cm^3 s^{-1} (STP denotes standard temperature 273.15 K and pressure 1 atm); total pressure ~86 Torr; T = 298 K. The efficiencies of photolysis of CH_2Br_2 are estimated to be ~5% based on the absorption cross section of $\sim 2.7 \times 10^{-19}$ cm^2 molecule^{-1} at 248 nm[26] and the laser fluence $\sim 1.9 \times 10^{17}$ photons cm^{-2}. CH_2Br_2 (99%, Alfa Aesar) and O_2 (99.999%) were used without further purification.

III. COMPUTATIONS

The equilibrium geometry, vibrational wavenumbers, IR intensities, and rotational parameters of $CH_2{}^{79}BrOO$ and $CH_2{}^{81}BrOO$ were calculated with the B3LYP density-functional theory using the Gaussian 09 program.[27] The B3LYP method uses Becke's three-parameter hybrid exchange functional with a correlation functional of Lee, Yang, and Parr.[28,29] Dunning's correlation-consistent polarized-valence triple-zeta basis set, augmented with s, p, d, and f functions (aug-cc-pVTZ)[30,31] was applied in these calculations. Analytic first derivatives were utilized in geometry optimization and vibrational wavenumbers were calculated analytically at each stationary point. The predictions of the corresponding anharmonic wavenumbers are also carried out by calculating the analytical second derivatives. Rotational parameters for each vibrational state ($v_i = 1$) were also calculated.

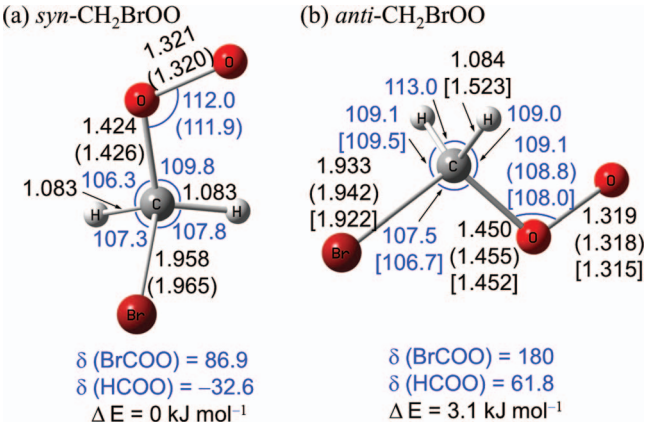

FIG. 1. Geometry of $CH_2{}^{79}BrOO$ calculated with the B3LYP/aug-cc-pVTZ method: (a) *syn*-CH_2BrOO and (b) *anti*-CH_2BrOO. The bond lengths in Å are indicated in black and the angles in degree are in blue. The results calculated by Lee *et al.*[32] with the B3LYP method and by Francisco and co-worker[33–35] with the MP2 method are shown in parenthesis and brackets, respectively. The C–H bond length of 1.523 Å (in bracket) might be a typing error in the original reference.

Geometries of CH_2BrOO calculated with the B3LYP/aug-cc-pVDZ and MP2/6-31G(d) methods have been reported;[32–35] they are compared with those calculated with the B3LYP/aug-cc-pVTZ method in Fig. 1. These predicted values deviate within 1% with previous results except the C–H bond length of *anti*-CH_2BrOO, which might be due to a typing error in previous reports.[33,34] Two stable conformers of CH_2BrOO exist. The *anti*-CH_2BrOO conformer was optimized with the C_s symmetry, but geometry optimization without symmetry restriction converged to the *syn*-CH_2BrOO conformer, which is 3.1 kJ mol^{-1} more stable than *anti*-CH_2BrOO. The Br–C–O–O dihedral angle of *syn*-CH_2BrOO is 86.9°, whereas the Br–C–O–O skeleton of *anti*-CH_2BrOO is planar. Compared with the corresponding bonds of *anti*-CH_2BrOO, *syn*-CH_2BrOO has a shorter C–O bond and a longer C–Br bond.[32] Rotational parameters for the equilibrium geometry, the vibrational ground state, and excited states ($v_i = 1$) of each vibrational mode of the two conformers of $CH_2{}^{79}BrOO$ were calculated with the B3LYP/aug-cc-pVTZ method; the ratios of A'/A'', B'/B'', and C'/C'', in which the prime and double primes indicate the vibrationally excited and ground states, respectively, are listed in Table I. The corresponding values of $CH_2{}^{81}BrOO$ are listed in Table SI of the supplementary material;[36] they are nearly the same as those of $CH_2{}^{79}BrOO$.

Harmonic and anharmonic vibrational wavenumbers, IR intensities, and approximate mode descriptions of *syn*-$CH_2{}^{79}BrOO$ predicted with the B3LYP/aug-cc-pVTZ method are listed in Table II; those of *anti*-$CH_2{}^{79}BrOO$ are listed in Table III. Corresponding values of $CH_2{}^{81}BrOO$ deviate from

TABLE I. Comparison of ratios of rotational parameters of *syn*-$CH_2{}^{79}BrOO$ and *anti*-$CH_2{}^{79}BrOO$ in their ground and vibrationally excited states predicted with the B3LYP/aug-cc-pVTZ method.

	syn-$CH_2{}^{79}BrOO$[a]			*anti*-$CH_2{}^{79}BrOO$[b]		
ν_i	A'/A''	B'/B''	C'/C''	A'/A''	B'/B''	C'/C''
ν_1	0.9979	1.0017	1.0012	0.9991	1.0008	1.0008
ν_2	0.9985	1.0005	1.0004	0.9974	1.0005	1.0005
ν_3	1.0015	0.9985	0.9993	0.9970	0.9994	1.0002
ν_4	0.9976	0.9990	0.9987	0.9966	0.9996	0.9983
ν_5	0.9961	1.0011	1.0006	0.9927	1.0005	1.0006
ν_6	0.9946	0.9992	0.9987	0.9992	0.9978	0.9982
ν_7	0.9949	1.0006	0.9996	1.0077	0.9968	0.9964
ν_8	1.0001	0.9946	0.9958	0.9865	0.9975	0.9975
ν_9	1.0017	0.9937	0.9945	0.9944	0.9968	0.9960
ν_{10}	0.9978	0.9997	0.9983	1.0095	0.9984	0.9983
ν_{11}	0.9991	0.9986	0.9986	1.0172	0.9998	0.9992
ν_{12}	1.0223	0.9957	0.9965	0.9494	1.0029	1.0053

[a]For *syn*-$CH_2{}^{79}BrOO$, $A'' = 0.5674\ cm^{-1}$, $B'' = 0.0731\ cm^{-1}$, $C'' = 0.0683\ cm^{-1}$ for $\nu = 0$ and $A_e'' = 0.5668\ cm^{-1}$, $B_e'' = 0.0738\ cm^{-1}$, $C_e'' = 0.0689\ cm^{-1}$ for the equilibrium geometry.
[b]For *anti*-$CH_2{}^{79}BrOO$, $A'' = 1.2051\ cm^{-1}$, $B'' = 0.0609\ cm^{-1}$, $C'' = 0.0587\ cm^{-1}$ for $\nu = 0$ and $A_e'' = 1.2373\ cm^{-1}$, $B_e'' = 0.0612\ cm^{-1}$, $C_e'' = 0.0589\ cm^{-1}$ for the equilibrium geometry.

those of $CH_2{}^{79}BrOO$ within 1 cm^{-1} so they are not listed. Bands of CH_2BrOO with anharmonic vibrational wavenumbers greater than 750 cm^{-1}, the lower limit of our spectral detection, are predicted at 3054 (ν_1), 2986 (ν_2), 1414 (ν_3), 1266 (ν_4), 1234 (ν_5), 1103 (ν_6), 944 (ν_7), and 858 (ν_8) cm^{-1} for *syn*-$CH_2{}^{79}BrOO$ and 3034 (ν_1), 2995 (ν_2), 1442 (ν_3), 1277 (ν_4), 1157 (ν_5), 1143 (ν_6), 887 (ν_7), and 883 (ν_8) cm^{-1} for *anti*-$CH_2{}^{79}BrOO$.

Predicted displacement vectors (thin arrows), the associated dipole derivatives (thick arrows), and the three rotational axes *a*, *b*, and *c* (arrows with dashed lines) for each vibrational mode of *syn*-$CH_2{}^{79}BrOO$ are available in Fig. S1 of the supplementary material.[36] The squares of the projections of dipole derivative onto the three rotational axis for each vibrational mode of CH_2BrOO determine the mixing ratios of bands of types *a*, *b*, and *c* in each transition.

TABLE II. Comparison of vibrational wavenumbers (in cm^{-1}) and IR intensities (in km mol^{-1}, listed parenthetically) for modes of *syn*-$CH_2{}^{79}BrOO$ derived from experiments and calculations with the B3LYP/aug-cc-pVTZ method.

		syn-$CH_2{}^{79}BrOO$		
ν_i	Mode	Harmonic	Anharmonic	Gas[a]
ν_1	C–H asym. str.	3203.2 (1)	3054.1	
ν_2	C–H sym. str.	3113.2 (4)	2985.8	
ν_3	CH_2 scissor	1451.4 (3)	1413.5	
ν_4	CH_2 wag	1293.6 (32)	1265.8	1276.1 (38)
ν_5	CH_2 twist	1261.9 (10)	1233.5	1243 (?)[b]
ν_6	O–O str.	1128.4 (16)	1103.3	1088.3 (18)
ν_7	CH_2 rock/C–O str.	965.2 (23)	943.6	961.0 (23)
ν_8	C–O str./CH_2 rock	886.6 (38)	858.1	884.9 (35)
ν_9	C–Br str.	603.9 (57)	609.9	
ν_{10}	COO in plane bend	508.9 (10)	500.3	
ν_{11}	COO out of plane bend	284.5 (1)	279.2	
ν_{12}	COO torsion	91.3 (1)	82.6	

[a]Integrated IR intensities relative to ν_7 mode of *syn*-CH_2BrOO are listed in parentheses.
[b]Tentative assignment because of small intensity.

TABLE III. Comparison of vibrational wavenumbers (in cm^{-1}) and IR intensities (in km mol^{-1}, listed parenthetically) for modes of *anti*-$CH_2{}^{79}BrOO$ derived from calculations with the B3LYP/aug-cc-pVTZ method.

		anti-$CH_2{}^{79}BrOO$		
ν_i	Mode	Harmonic	Anharmonic	Gas[a]
ν_1	C–H asym. str.	3189.2 (0)	3033.9	
ν_2	C–H sym. str.	3105.4 (2)	2994.8	
ν_3	CH_2 scissor	1467.0 (4)	1442.3	
ν_4	CH_2 wag	1305.7 (63)	1276.6	1277.0? (10)[b]
ν_5	CH_2 twist	1189.1 (3)	1157.2	
ν_6	O–O str.	1159.6 (14)	1143.2	
ν_7	C–O str.	930.9 (20)	886.8	
ν_8	CH_2 rock	897.9 (0)	882.8	
ν_9	C–Br str.	710.5 (78)	695.8	
ν_{10}	COO bend	380.0 (3)	379.1	
ν_{11}	BrCO bend	235.9 (2)	234.1	
ν_{12}	COO torsion	50.8 (2)	40.9	

[a]Integrated IR intensities relative to ν_7 mode of *syn*-CH_2BrOO are listed in parentheses.
[b]Tentative assignment because of overlap with the ν_4 mode of *syn*-CH_2BrOO; see text.

IV. RESULTS AND DISCUSSION

Although previous researchers on UV absorption experiments used the reaction of F or Cl with CH_3Br to generate CH_2Br for its reaction with O_2, we employed photolysis of CH_2Br_2 as the source of CH_2Br because of its ease of operation and less interference. As a test, conventional FTIR measurements were performed with a static cell containing CH_2Br_2 (1.2 Torr) and O_2 (87 Torr). The end products were identified as H_2CO (at 1500, 1746, and 2782 cm^{-1}), H(Br)CO (at 1271 and 1798 cm^{-1}),[37] HBr (at 2550 cm^{-1}), CO (at 2140 cm^{-1}), and CO_2 (at 2349 cm^{-1}). These end products except CO_2 agree with those obtained by UV photolysis of a mixture of CH_3Br (1 Torr) and Cl_2 (0.5 Torr) in 700 Torr of air.[18]

A. Photolysis of CH_2Br_2 in O_2

To avoid the interference from internally excited reactants and products, we employed excessive O_2 in the reactor to serve as both a reactant and a quencher to thermalize CH_2Br_2, CH_2BrOO, and other products upon UV irradiation. Representative survey spectra (resolution 4 cm^{-1}) recorded before and after irradiation, with an excimer laser at 248 nm, of a flowing mixture of CH_2Br_2 (0.25 Torr), N_2 (0.60 Torr), and O_2 (85.1 Torr) at 298 K are shown in Figs. 2(a)–2(e), respectively. Difference spectra were recorded after irradiation; traces (b)–(d) were recorded at 25-μs intervals, whereas trace (e) was recorded during 250–275 μs after irradiation. In these difference spectra, features pointing upward indicate production, whereas those pointing downward indicate destruction. The downward features of the parent compound, near 1195 cm^{-1}, are due to destruction of CH_2Br_2 upon irradiation. New features in a group near 885, 960, 1090, and 1275 cm^{-1},

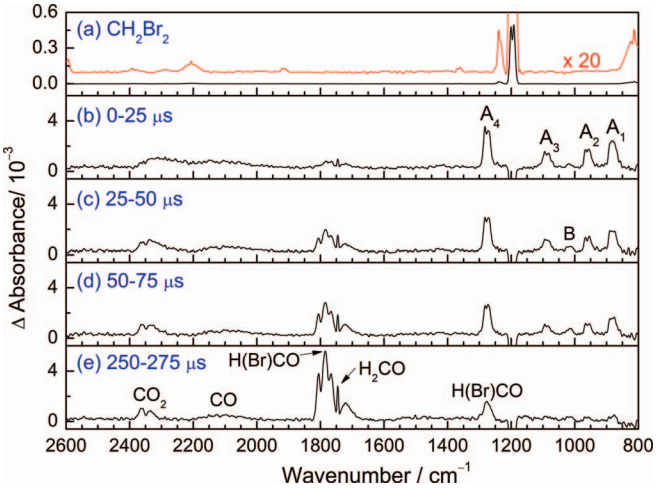

FIG. 2. Survey spectra of transient differential absorption spectra recorded upon 248-nm photolysis of a flowing mixture of $CH_2Br_2/O_2/N_2$ (~1/2.4/340, 86 Torr, 298 K). Path length is 3.6 m; resolution is 4.0 cm^{-1}. (a) Spectrum of CH_2Br_2 before irradiation. (b)–(e) Spectra recorded 0–25, 25–50, 50–75, and 250–275 μs after irradiation; bands in group A and B are indicated.

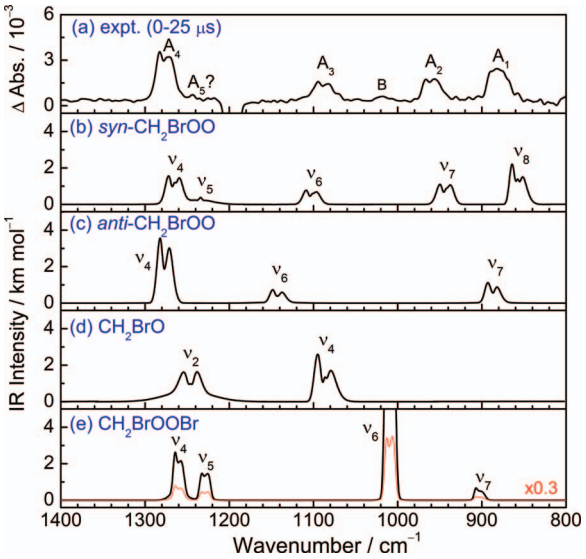

FIG. 3. Comparison of the observed spectrum with simulated spectra of possible candidates. (a) Difference absorption spectrum recorded 0–25 μs after 248-nm photolysis of a flowing mixture of $CH_2Br_2/O_2/N_2$ (~1/2.4/340, 86 Torr, 298 K); IR spectra of *syn*-CH_2BrOO (b), *anti*-CH_2BrOO (c), CH_2BrO (d), and $CH_2BrOOBr$ (e) simulated with rotational parameters, vibrational wavenumbers, and IR intensities predicted with the B3LYP/aug-cc-pVTZ method. The integrated absorbance of predicted bands represents the predicted IR intensities.

designated group A, appeared immediately upon irradiation and decayed rapidly with a decay time constant ~130 μs. The feature near 1015 cm^{-1}, designated as B, showed temporal behavior distinct from features in group A; it increased in intensity to reach its maximum near 90 μs, followed by a slower decay with a decay constant ~180 μs. Lines of H(Br)CO (near 1798 cm^{-1}) and H_2CO (near 1746 cm^{-1}) increased in intensity gradually. Weak absorption of internally excited CO_2 and CO appeared immediately upon UV irradiation and became thermalized near 150 μs.

B. Assignments of bands A1–A4 to CH_2BrOO

The major product on photolysis of CH_2Br_2 was reported to be CH_2Br;[38] CH_2Br subsequently reacts with O_2 to form CH_2BrOO,[9,10]

$$CH_2Br + O_2 + M \rightarrow CH_2BrOO + M, \quad (3)$$

with a rate coefficient of $k_3(T) = 1.2 \times 10^{-30}\ (T/300)^{-4.8}$ cm^6 $molecule^{-2}$ s^{-1} for the termolecular reaction with M = He in the temperature range of 241–363 K.[9] At 298 K and 86 Torr, this reaction is expected to be completed within 1 μs. Although the reaction of CH_2I with O_2 produces the important Criegee intermediate CH_2OO, the corresponding reaction,

$$CH_2Br + O_2 \rightarrow CH_2OO + Br, \quad (4)$$

is endothermic by 51 kJ mol^{-1};[10,32] the reaction might proceed only when CH_2Br has enough applicable energy to overcome the barrier of height ~51 kJ mol^{-1}.[10,32] The observed bands in group A disagree with those observed for CH_2OO because the IR spectrum of gaseous CH_2OO has been well characterized,[22] with vibrational wavenumbers $\nu_3 = 1435$, $\nu_4 = 1286$, $\nu_5 = 1241$, $\nu_6 = 908$, and $\nu_8 = 848$ cm^{-1}.

Possible secondary reactions in this system are

$$CH_2BrOO + CH_2BrOO \rightarrow 2CH_2BrO + O_2 \text{ and other products}, \quad (1')$$

$$CH_2BrO \rightarrow H_2CO + Br, \quad (2')$$

$$CH_2BrOO + CH_2Br \rightarrow CH_2BrO + CH_2BrO, \quad (5)$$

$$CH_2BrOO + Br \rightarrow CH_2BrOOBr. \quad (6)$$

The rate coefficient of reaction (1′) is reported to be $k_1 = 1.1 \times 10^{-12}$ cm^3 $molecule^{-1}$ s^{-1} at 298 K (Ref. 11) and reaction (2′) is reported to occur rapidly.[18,19] We thus expect that, in addition to CH_2BrOO, other possible species responsible for the observed new features might be CH_2BrO and $CH_2BrOOBr$. IR spectra of *syn*-CH_2BrOO and *anti*-CH_2BrOO in the region 800–1400 cm^{-1} simulated with anharmonic vibrational wavenumbers, IR intensities, and rotational parameters predicted with the B3LYP/aug-cc-pVTZ method are shown in Figs. 3(b) and 3(c), respectively; simulation of rotational contours is discussed later. IR spectra of CH_2BrO and $CH_2BrOOBr$ simulated with the same method are shown in Figs. 3(d) and 3(e), respectively; the parameters used are listed in Table SII of the supplementary material.[36]

Bands observed near 885, 960, 1090, and 1275 cm^{-1} clearly agree satisfactorily with those predicted at 858, 944, 1103, and 1266 cm^{-1} for *syn*-CH_2BrOO, with deviations less than 3%. The ν_5 band predicted at 1234 cm^{-1} might correspond to a weak band near 1243 cm^{-1}, but its identification is uncertain because of its small intensity. The contribution of *anti*-CH_2BrOO is expected to be small because of its higher energy, but its presence cannot be positively excluded because its ν_6 and ν_7 bands are predicted to be weak, and the intense ν_4 band might be overlapped with that of *syn*-CH_2BrOO. Predicted bands of CH_2BrO and $CH_2BrOOBr$ disagree with our observations for neither band position nor rotational contour.

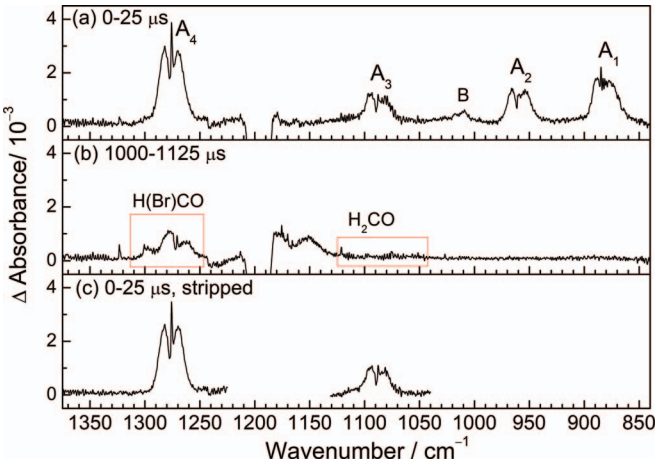

FIG. 4. Temporally resolved spectra at resolution 0.5 cm^{-1} in the range 840–1375 cm^{-1} recorded upon photolysis at 248 nm of a flowing mixture of $CH_2Br_2/O_2/N_2$ (~1/2.4/340, 86 Torr, 298 K). Spectra recorded at 0–25 μs (a) and 1000–1125 μs (b) after photolysis. (c) Spectrum with absorption of H_2CO and H(Br)CO stripped; see text for details.

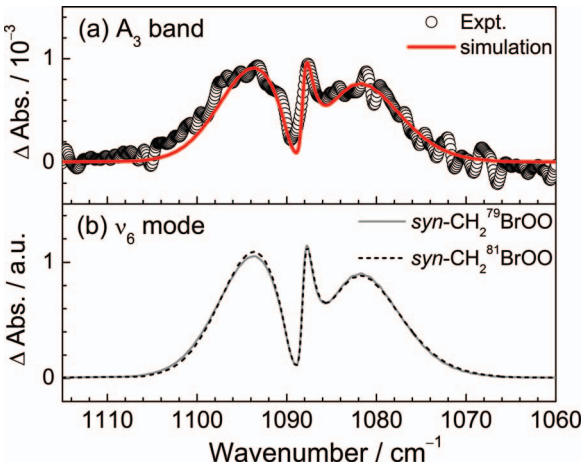

FIG. 5. Comparison of band A_3 with the spectrum simulated for the ν_6 mode of *syn*-CH_2BrOO in region 1060–1115 cm^{-1} at resolution 0.5 cm^{-1}. (a) Experimental data (open circles) and resultant simulated spectrum (thick line). (b) Individual simulated bands for *syn*-$CH_2{}^{79}BrOO$ ($\nu_6 = 1088.3$ cm^{-1}) and *syn*-$CH_2{}^{81}BrOO$ ($\nu_6 = 1088.3$ cm^{-1}).

To support further the assignments of bands in group A to *syn*-CH_2BrOO, we recorded the spectra under similar experimental condition at instrument resolution 0.5 cm^{-1} (effective FWHM 0.64 cm^{-1}) and simulated the band contour using the molecular parameters predicted with the B3LYP/aug-cc-pVTZ method for comparison. No experiment with higher resolution was attempted because the rotational parameters of CH_2BrOO are small and partial resolution of the rotational structures with our current setup is unlikely. Figs. 4(a) and 4(b) show the spectra recorded 0–25 and 1000–1125 μs after laser irradiation, respectively. As the observed bands A_3 and A_4 in Fig. 4(a) near 1090 and 1275 cm^{-1} are overlapped with the absorption of H_2CO and H(Br)CO, respectively, the contributions from these two species were separately subtracted by spectral stripping of the corresponding bands of H_2CO and H(Br)CO shown in Fig. 4(b) to yield the corrected spectrum shown in Fig. 4(c).

With the PGopher program,[39] we simulated the spectrum of each band using predicted ratios of rotational parameters A', A'', B', B'', C', and C'' (listed in Table I), $J_{max} = 140$, $T = 298$ K, and a Gaussian width 0.64 cm^{-1}. Simulated *a*-, *b*-, and *c*-type spectra for ν_4, ν_6–ν_8 of *syn*-CH_2BrOO are shown in Fig. S2 of the supplementary material.[36] The projections of the dipole derivatives for each vibrational mode of *syn*-CH_2BrOO, shown in Fig. S1 of the supplementary material,[36] onto rotational axes *a*, *b*, and *c* determine the weighting of bands of types *a*, *b*, and *c* in each vibrational absorption band. The resultant rotational contours according to these weighting factors are shown also as the bottom trace for each vibrational band in Fig. S2 of the supplementary material.[36]

The corrected A_3 band near 1090 cm^{-1} recorded 0–25 μs upon irradiation at resolution 0.5 cm^{-1} is shown in Fig. 5(a) with open circles and compared with the O–O stretching (ν_6) band, simulated for *syn*-$CH_2{}^{79}BrOO$ and *syn*-$CH_2{}^{81}BrOO$ with predicted spectral parameters, as shown in Fig. 5(b). This band is mostly *a*-type with a significant Q branch; the weighting of types is *a*: *b*: *c* = 0.75:0.11:0.14. The difference between the simulated bands of *syn*-$CH_2{}^{79}BrOO$ and *syn*-$CH_2{}^{81}BrOO$ is negligibly small. Using a population ratio of *syn*-$CH_2{}^{79}BrOO$: *syn*-$CH_2{}^{81}BrOO$ = 50.7:49.3, the resultant simulated spectrum is shown as a solid curve in Fig. 5(a); it agrees satisfactorily with experiments. The fitted vibrational wavenumber is $\nu_6 = 1088.3$ cm^{-1}.

The observed A_1 band near 885 cm^{-1} recorded, at resolution 0.5 cm^{-1}, 0–25 μs upon irradiation (open circles, Fig. 6(a)) is compared with the ν_8 band simulated for *syn*-$CH_2{}^{79}BrOO$ and *syn*-$CH_2{}^{81}BrOO$ with predicted spectral parameters (Fig. 6(b)); this mode is approximately described as the C–O stretching mode coupled with the CH_2-rocking mode. This band is mostly *a*-type with a weighting factor of types *a*: *b*: *c* = 0.92:0.02:0.06. Similarly to ν_6, the simulated bands of *syn*-$CH_2{}^{79}BrOO$ and *syn*-$CH_2{}^{81}BrOO$ are nearly identical. Using a population ratio of *syn*-$CH_2{}^{79}BrOO$: *syn*-$CH_2{}^{81}BrOO$ = 50.7:49.3, the resultant simulated spectrum is shown as a solid curve in Fig. 6(a), which differs significantly from our experimental observation. We noticed a series of Q-bands in the structure of the observed spectrum and suggest that this series might be contributed by hot bands from levels of the low-energy vibrational mode. The smallest vibrational wavenumber of *syn*-CH_2BrOO is predicted to be 83 cm^{-1} for the torsional (ν_{12}) mode. We located the positions of the first four Q-bands in the observed spectrum, and consequently assumed that the shifts for additional bands from absorption initiated from vibrationally excited levels of ν_{12} due to anharmonicity are regular, the contours of the hot bands are similar to that of the fundamental, and the population distributions of these excited levels of ν_{12} are Boltzmann. We obtained a satisfactory fit of our observed spectrum to a simulated spectrum comprising the fundamental and ten additional hot bands, $8_0^1 12_v^v$ with v = 0–10. The contribution of each component is shown in Fig. 6(d) and the resultant spectrum (solid line) is compared with experimental observation in Fig. 6(c). The fitted fundamental vibrational wavenumber of ν_8 is 884.9 cm^{-1}; the peak positions and relative populations of other components are presented in Table IV.

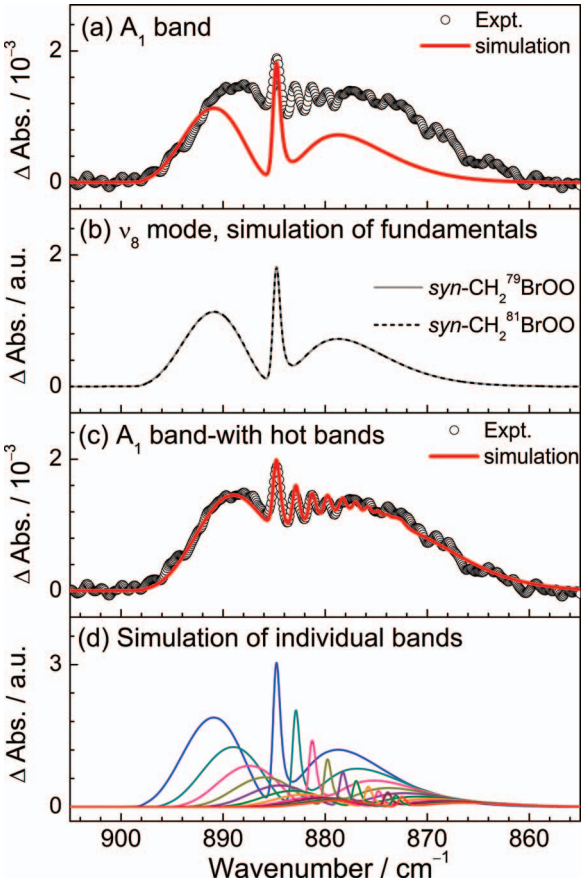

FIG. 6. Comparison of band A_1 with the spectrum simulated for the ν_8 mode of *syn*-CH_2BrOO in region 855–905 cm^{-1} at resolution 0.5 cm^{-1}. (a) Experimental data (open circles) and resultant simulated spectrum (thick line). (b) Individual simulated bands for *syn*-$CH_2{}^{79}BrOO$ (ν_8 = 884.9 cm^{-1}) and *syn*-$CH_2{}^{81}BrOO$ (ν_8 = 884.9 cm^{-1}). (c) Experimental data (open circles) and resultant simulated spectrum (thick line) including hot bands; see text. (d) Individual simulated bands for *syn*-CH_2BrOO (ν_8 = 884.9 cm^{-1}); the band origins and relative intensities are listed in Table IV.

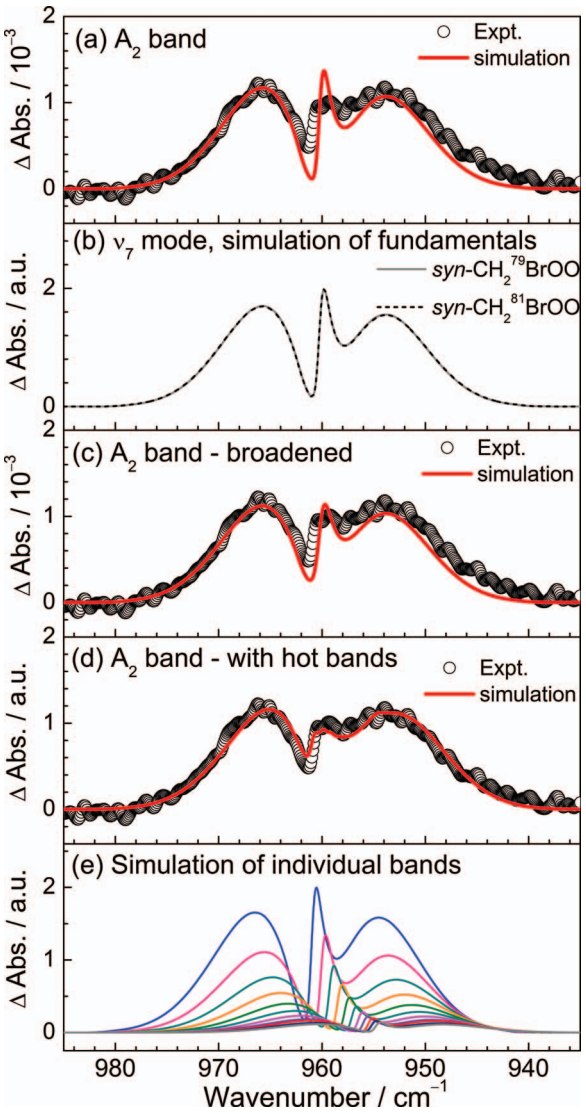

FIG. 7. Comparison of band A_2 with the spectrum simulated for the ν_7 mode of *syn*-CH_2BrOO in region 935–985 cm^{-1} at resolution 0.5 cm^{-1}. (a) Experimental data (open circles) and resultant simulated spectrum (thick line). (b) Individual simulated bands for *syn*-$CH_2{}^{79}BrOO$ (ν_7 = 960.3 cm^{-1}) and *syn*-$CH_2{}^{81}BrOO$ (ν_7 = 960.3 cm^{-1}). (c) Experimental data (open circles) and resultant simulated spectrum (thick line) using an additional Lorentzian width of 0.5 cm^{-1}; see text. (d) Experimental data (open circles) and resultant simulated spectrum (thick line) including hot bands; see text. (e) Individual simulated bands for *syn*-CH_2BrOO (ν_7 = 961.0 cm^{-1}); the band origins and relative intensities are listed in Table IV.

The observed A_2 band near 960 cm^{-1} recorded 0–25 μs upon irradiation at resolution 0.5 cm^{-1} (open circles, Fig. 7(a)) is compared with the ν_7 band simulated for *syn*-$CH_2{}^{79}BrOO$ and *syn*-$CH_2{}^{81}BrOO$ with predicted spectral parameters (Fig. 7(b)); this mode is approximately described as the CH_2-rocking mode coupled with C–O stretching mode. This band is mostly type *a* with a significant Q branch; the weighting of types *a*: *b* is 0.98:0.02. Similarly to ν_6, no difference between the simulated bands of *syn*-$CH_2{}^{79}BrOO$ and *syn*-$CH_2{}^{81}BrOO$ is discernible; the simulation of these two bands with origins both at 960.3 cm^{-1} and a population ratio of $CH_2{}^{79}BrOO$:$CH_2{}^{81}BrOO$ = 50.7:49.3 yielded a spectrum shown as a solid curve in Fig. 7(a), which shows some small deviations from the experimental results. The Q-branch in the experimental spectrum is smaller and broader than the simulated one. We consider that this effect might be due to (1) a slightly greater width needed for the simulated spectrum or (2) contributions of hot bands from ν_{12}. The simulated

TABLE IV. Band origins and relative populations of the fundamental and hot bands of $7_0^1 12_v^v$ and $8_0^1 12_v^v$.

	Band origin (cm^{-1})		
v	$7_0^1 12_v^v$	$8_0^1 12_v^v$	Relative population
0	961.0	884.9	1.00
1	960.1	883.0	0.67
2	959.3	881.4	0.46
3	958.5	879.9	0.33
4	957.8	878.4	0.24
5	957.1	877.1	0.18
6	956.5	875.9	0.14
7	956.0	874.9	0.11
8	955.5	874.0	0.10
9	955.2	873.2	0.08
10	954.8	872.6	0.07

spectrum with additional Lorentzian width of 0.5 cm^{-1} (solid line) is compared with experimental results (open circle); the agreement became improved, as illustrated in Fig. 7(c). We tried also to simulate the spectrum by considering hot bands of $7_0^1 12_v^v$ with a smaller anharmonic shift (50% of the spacing of $8_0^1 12_v^v$ hot bands) and a similar Boltzmann distribution as $8_0^1 12_v^v$. The resultant simulation with a fitted fundamental vibrational wavenumber 961.0 cm^{-1} of ν_7 is shown as a solid curve in Fig. 7(d), which also agrees with the experimental spectrum. The contribution of each component is shown in Fig. 7(e); the fitted peak positions of individual bands are presented in Table IV.

The observed A_4 band near 1275 cm^{-1} recorded at 0.5 cm^{-1} resolution and 0–25 μs (open circles, Fig. 8(a)) is compared with the ν_4 band simulated for *syn*-$CH_2{}^{79}BrOO$ and *syn*-$CH_2{}^{81}BrOO$ with predicted spectral parameters. This band, approximately described as the CH_2-wagging mode, is mostly *a*-type with a significant Q branch and a weighting factor types *a*: *b*: *c* = 0.78:0.20:0.02. Similarly to other modes, no difference between the simulated bands of *syn*-$CH_2{}^{79}BrOO$ and *syn*-$CH_2{}^{81}BrOO$ (thin lines in Fig. 8(a)) is discernible. The resultant simulated spectrum from these two isotopologues is shown as a thick solid line in Fig. 8(a), which shows some deviations from our experimental result. The most intense band (ν_4) of *anti*-CH_2BrOO (1277 cm^{-1}) was predicted to have anharmonic vibrational wavenumber

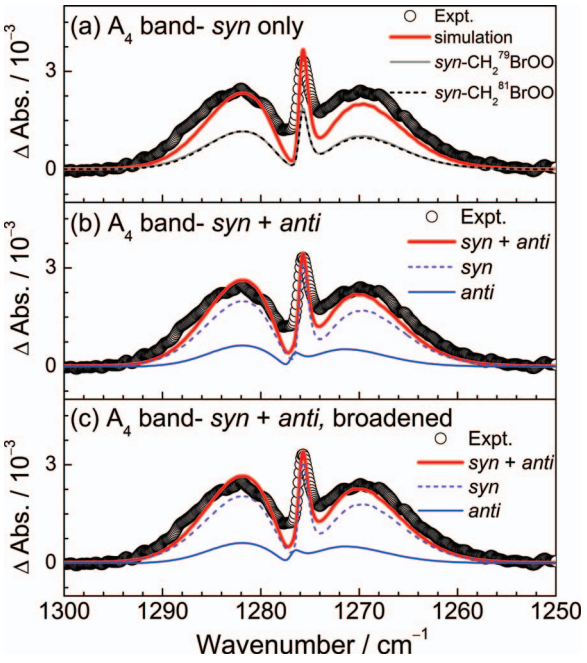

FIG. 8. Comparison of band A_4 with the spectrum simulated for the ν_4 mode of *syn*-CH_2BrOO in region 1250–1300 cm^{-1} at resolution 0.5 cm^{-1}. (a) Experimental data (open circles) and resultant simulated spectrum (thick line); individual simulated bands for *syn*-$CH_2{}^{79}BrOO$ (ν_4 = 1276.1 cm^{-1}) and *syn*-$CH_2{}^{81}BrOO$ (ν_7 = 1276.1 cm^{-1}) are shown with thin lines. (b) Experimental data (open circles) and resultant simulated spectrum (thick line) with an additional band of *anti*-CH_2BrOO; individual simulated bands for *syn*-CH_2BrOO (ν_4 = 1276.1 cm^{-1}) and *anti*-CH_2BrOO (ν_4 = 1277.0 cm^{-1}) are shown with thin lines. (c) Experimental data (open circles) and resultant simulated spectrum (thick line) with an additional band of *anti*-CH_2BrOO using an Lorentzian width of 0.2 cm^{-1}; individual simulated bands for *syn*-CH_2BrOO (ν_4 = 1276.1 cm^{-1}) and *anti*-CH_2BrOO (ν_4 = 1277.0 cm^{-1}) are shown with thin lines; see text.

11 cm^{-1} greater and intensity twice more than that of *syn*-CH_2BrOO (1266 cm^{-1}). If the predicted energy difference of 3.1 kJ mol^{-1} is correct, we expect the population ratio of *anti*-CH_2BrOO: *syn*-CH_2BrOO to be 0.14:1.00 at 298 K, assuming a Boltzmann distribution. We simulated the spectra on adding the ν_4 bands of both *syn*- and *anti*-CH_2BrOO with the band origin of *anti*-CH_2BrOO varied from 1273 to 1280 cm^{-1} to search for the best fit. The best simulated spectrum (thick line in Fig. 8(b)) with the ν_4 modes of *syn*-CH_2BrOO at 1276.1 cm^{-1} and that of *anti*-CH_2BrOO at 1277.0 cm^{-1} (thin line in Fig. 8(b)) is shown as thick line in Fig. 8(b); the agreement is improved. We simulated also the spectrum on considering slightly Lorentzian-broadened (L = 0.2 cm^{-1}) *anti*-CH_2BrOO with the ν_4 mode of *syn*-CH_2BrOO at 1276.1 cm^{-1} and that of *anti*-CH_2BrOO at 1277.0 cm^{-1} having a ratio of *anti*-CH_2BrOO: *syn*-CH_2BrOO = 0.13:1.00. The resultant simulation is shown as a solid curve in Fig. 8(c), which agrees best with the experimental spectrum. Hence we assign the observed A_4 band to the CH_2-wagging mode of *syn*-CH_2BrOO, with a possibility of a small contribution of *anti*-CH_2BrOO. As the intensities of other bands of *anti*-CH_2BrOO (ν_6 and ν_7) are much smaller, they could not be observed with the current ratio of signal to noise.

For all 12 vibrational modes of *syn*-CH_2BrOO, eight modes are within our detection range (>750 cm^{-1}); we detected the four most intense modes; the fifth mode predicted near 1234 cm^{-1} (ν_5) might have been observed near 1243 cm^{-1} (Fig. 3(a)), but the intensity was too small for a positive identification. The other three unobserved modes have predicted IR intensities less than 4 km mol^{-1}. The observed vibrational wavenumbers and relative IR intensities are compared with theoretical computations in Table II; the deviations between observed wavenumbers and predicted anharmonic vibrational wavenumbers are less than 27 cm^{-1} (3%); the agreements in relative IR intensities are satisfactory.

The peroxy radicals that we observed all have similar O–O stretching wavenumbers; CH_3OO,[23] *cis*-$CH_3C(O)OO$,[24] *trans*-$CH_3C(O)OO$,[24] $C_6H_5C(O)OO$,[25] and CH_3SOO[40] absorb at 1117 ± 2, 1078 ± 6, 1102 ± 3, 1108 ± 4, and 1110 ± 3 cm^{-1}, respectively, even though some modes are mixed with other vibrations. The IR spectra of other methyl halogenated peroxy radicals have also been observed. The reported O–O stretching and C–O stretching wavenumbers for CH_2ClOO in Ar matrix are 1088.2 and 884.6 cm^{-1}.[41] The corresponding wavenumbers for CH_2IOO in *p*-H_2 matrix are 1085.6 and 917.7 cm^{-1}.[42] These results agree with the corresponding values of 1088.3 cm^{-1} and 884.9/961.0 cm^{-1} that we observed.

C. Possible assignment of band B to $CH_2BrOOBr$

As discussed previously, the intensity of band B increased to a maximum near 90 μs, followed by a decay with a decay constant ~180 μs. When the concentration of CH_2Br_2 was increased, the period for band B to reach its maximum decreased, indicating that the carrier was formed from secondary reactions involving CH_2Br or Br.

As discussed in Sec. IV B, CH_2Br and Br were the main products upon irradiation of CH_2Br_2; CH_2Br reacted readily

with excessive O_2 in the flow system to produce CH_2BrOO. The most likely products of secondary reactions are CH_2BrO, H_2CO, and $CH_2BrOOBr$. The simulated spectra of CH_2BrO and $CH_2BrOOBr$ appear in Figs. 3(d) and 3(e), respectively. The most intense band of $CH_2BrOOBr$ in Fig. 3(e) agrees satisfactorily with the experimental observation; the intensities of the other three bands of $CH_2BrOOBr$ predicted near 1261, 1229, and 904 cm^{-1} are too small to be observed. As the small intensity precludes reliable comparison of rotational contours, the assignment is tentative.

Similarly, we observed also three absorption bands of $C_6H_5C(O)Br$ near 1793, 1176, and 1195 cm^{-1} when we photolyzed a mixture of C_6H_5Br and CO; $C_6H_5C(O)Br$ was produced from a secondary reaction of C_6H_5CO with Br, which was produced also upon photolysis of precursor C_6H_5Br.[43]

V. CONCLUSION

We observed four transient IR bands of the bromomethyl peroxy radical CH_2BrOO upon photolysis of gaseous CH_2Br_2 in O_2 using a step-scan Fourier-transform infrared absorption spectrometer; the IR spectrum of CH_2BrOO is previously unreported. Bands with origins at 1276.1, 1088.3, 961.0, and 884.9 cm^{-1}, assigned to ν_4 (CH_2-wagging), ν_6 (O–O stretching), ν_7 (CH_2-rocking mixed with C–O stretching), and ν_8 (C–O stretching mixed with CH_2-rocking) modes of *syn*-CH_2BrOO, respectively, and their relative IR intensities agree with those predicted with the B3LYP/aug-cc-pVTZ method. A weak band near 1243 cm^{-1} might be assigned to the CH_2 twisting (ν_5) mode. Observed rotational contours of these bands also conform satisfactorily to those simulated according to rotational parameters derived from quantum-chemical calculations. The rotational contours of ν_7 and ν_8 indicate that hot bands involving ν_{12} are also present, with transitions $7_0^1 12_v^v$ and $8_0^1 12_v^v$, $v = 1$–10. The possibility that the most intense band of *anti*-CH_2BrOO near 1277 cm^{-1} might have a small contribution cannot be excluded. An additional weak band near 1015 cm^{-1}, observed at a later period after laser irradiation, is assigned to $CH_2BrOOBr$ that was produced from a secondary reaction of CH_2BrOO with Br. Our work provides information for directly probing gaseous CH_2BrOO with IR spectroscopy, in either the atmosphere or laboratory experiments.

ACKNOWLEDGMENTS

Ministry of Science and Technology (Grant No. MOST103-2745-M-009-001-ASP) and Ministry of Education, Taiwan ("Aim for the Top University Plan" of National Chiao Tung University) supported this work. The National Center for High-Performance Computation provided computer time.

[1] Q. Liang, R. S. Stolarski, S. R. Kawa, J. E. Nielsen, A. R. Douglass, J. M. Rodriguez, D. R. Blake, E. L. Atlas, and L. E. Ott, Atmos. Chem. Phys. **10**, 2269 (2010).
[2] S. Tegtmeier, K. Krüger, B. Quack, E. L. Atlas, I. Pisso, A. Stohl, and X. Yang, Atmos. Chem. Phys. **12**, 10633 (2012).
[3] R. Tokarczyk and R. M. Moore, Geophys. Res. Lett. **21**, 285, doi:10.1029/94GL00009 (1994).
[4] K. Toyota, Y. Kanaya, M. Takahashi, and H. Akimoto, Atmos. Chem. Phys. **4**, 1961 (2004).
[5] N. J. Warwick, J. A. Pyle, G. D. Carver, X. Yang, N. H. Savage, F. M. O'Connor, and R. A. Cox, J. Geophys. Res. **111**, D24305, doi:10.1029/2006JD007264 (2006).
[6] S. M. Schauffler, E. L. Atlas, D. R. Blake, F. Flocke, R. A. Lueb, J. M. Lee-Taylor, V. Stroud, and W. Travnicek, J. Geophys. Res. **104**, 21513, doi:10.1029/1999JD900197 (1999).
[7] A. Mellouki, R. K. Talukdar, A.-M. Schmoltner, T. Gierczak, M. J. Mills, S. Solomon, and A. R. Ravishankara, Geophys. Res. Lett. **19**, 2059, doi:10.1029/92GL01612 (1992).
[8] J. J. Orlando, G. S. Tyndall, T. J. Wallington, and M. Dill, Int. J. Chem. Kinet. **28**, 433 (1996).
[9] A. J. Eskola, D. Wojcik-Pastuszka, E. Ratajczak, and R. S. Timonen, Phys. Chem. Chem. Phys. **8**, 1416 (2006).
[10] W. S. McGivern, H. Kim, J. S. Francisco, and S. W. North, J. Phys. Chem. A **108**, 7247 (2004).
[11] E. Villenave and R. Lesclaux, Chem. Phys. Lett. **236**, 376 (1995).
[12] O. J. Nielsen, J. Munk, G. Locke, and T. J. Wallington, J. Phys. Chem. **95**, 8714 (1991).
[13] J. Sehested, O. J. Nielsen, and T. J. Wallington, Chem. Phys. Lett. **213**, 457 (1993).
[14] J. C. McConnell, G. S. Henderson, L. Barrie, J. Bottenheim, H. Niki, C. H. Langford, and E. M. J. Templeton, Nature (London) **355**, 150 (1992).
[15] P. O. Wennberg, R. C. Cohen, R. M. Stimpfle, J. P. Koplow, J. G. Anderson, R. J. Salawitch, D. W. Fahey, E. L. Woodbridge, E. R. Keim, R. S. Gao, C. R. Webster, R. D. May, D. W. Toohey, L. M. Avallone, M. H. Proffitt, M. Loewenstein, J. R. Podolske, K. R. Chan, and S. C. Wofsy, Science **266**, 398 (1994).
[16] D. J. Lary, J. Geophys. Res. **102**, 21515, doi:10.1029/97JD00912 (1997).
[17] J. Sehested, M. Bilde, T. Møgelberg, T. J. Wallington, and O. J. Nielsen, J. Phys. Chem. **100**, 10989 (1996).
[18] J. Chen, V. Catoire, and H. Niki, Chem. Phys. Lett. **245**, 519 (1995).
[19] J. J. Orlando, G. S. Tyndall, and T. J. Wallington, J. Phys. Chem. **100**, 7026 (1996).
[20] C.-Y. Chung, C.-W. Cheng, Y.-P. Lee, H.-Y. Liao, E. N. Sharp, P. Rupper, and T. A. Miller, J. Chem. Phys. **127**, 044311 (2007).
[21] Y.-H. Huang, J.-D. Chen, K.-H. Hsu, L.-K. Chu, and Y.-P. Lee, J. Chin. Chem. Soc. **61**, 47 (2014).
[22] Y.-T. Su, Y.-H. Huang, H. A. Witek, and Y.-P. Lee, Science **340**, 174 (2013).
[23] D.-R. Huang, L.-K. Chu, and Y.-P. Lee, J. Chem. Phys. **127**, 234318 (2007).
[24] S.-Y. Chen and Y.-P. Lee, J. Chem. Phys. **132**, 114303 (2010).
[25] B. Golec, J.-D. Chen, and Y.-P. Lee, J. Chem. Phys. **135**, 224302 (2011).
[26] L. T. Molina, M. J. Molina, and F. S. Rowland, J. Phys. Chem. **86**, 2672 (1982).
[27] M. J. Frisch, G. W. Trucks, H. B. Schlegel *et al.*, Gaussian 09, Revision 7.0, Gaussian, Inc., Wallingford, CT, 2009.
[28] A. D. Becke, J. Chem. Phys. **98**, 5648 (1993).
[29] C. Lee, W. Yang, and R. G. Parr, Phys. Rev. B **37**, 785 (1988).
[30] T. H. Dunning, J. Chem. Phys. **90**, 1007 (1989).
[31] D. E. Woon and T. H. Dunning, Jr., J. Chem. Phys. **98**, 1358 (1993).
[32] E. P. F. Lee, D. K. W. Mok, D. E. Shallcross, C. J. Percival, D. L. Osborn, C. A. Taatjes, and J. M. Dyke, Chemistry **18**, 12411 (2012).
[33] M. Martínez-Avilés, C. M. Rosado-Reyes, and J. S. Francisco, J. Phys. Chem. A **111**, 11652 (2007).
[34] M. Martínez-Avilés, C. M. Rosado-Reyes, and J. S. Francisco, J. Phys. Chem. A **112**, 7930 (2008).
[35] C. J. Christiansen and J. S. Francisco, J. Phys. Chem. A **113**, 7189 (2009).
[36] See supplementary material at http://dx.doi.org/10.1063/1.4897982 for comparison of rotational parameters of *syn*-$CH_2{}^{81}BrOO$, *anti*-$CH_2{}^{81}BrOO$, CH_2BrO, and $CH_2BrOOBr$ in their ground and vibrationally excited states, the predicted displacement vectors and directions of dipole derivatives for all vibrational modes of *syn*-CH_2BrOO, and the simulated rotational contours for ν_4 and ν_6-ν_8 modes of *syn*-CH_2BrOO.
[37] G. Yarwood, H. Niki, and P. Maker, J. Phys. Chem. **95**, 4773 (1991).
[38] Y.-R. Lee, C.-C. Chen, and S.-M. Lin, J. Chem. Phys. **118**, 10494 (2003).
[39] C. M. Western, PGOPHER, a program for simulating rotational structure, University of Bristol, version 7.1.108, 2010, http://pgopher.chm.bris.ac.uk.
[40] L.-K. Chu and Y.-P. Lee, J. Chem. Phys. **133**, 184303 (2010).
[41] M. Zhou, R. Ma, D. Yuan, and M. Chen, J. Phys. Chem. A **113**, 2826 (2009).
[42] Y.-F. Lee and Y.-P. Lee, private communication (2014).
[43] S.-Y. Lin and Y.-P. Lee, J. Phys. Chem. A **116**, 6366 (2012).